S1 CFD model construction and pre-processing

Figure S1: Vehicle geometry reconstruction based on UAV-mounted LiDAR measurements.

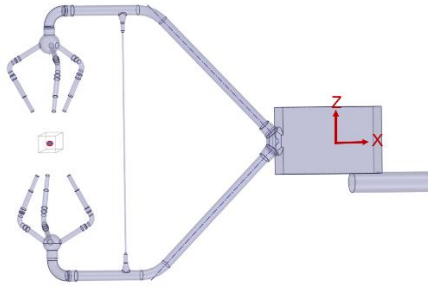

Figure S2: Schematic of the anemometer control volume.

S2 Overview of the field validation experiment

Table S1: Overview of daily data acquisition during the wind correction validation experiment.

Date	Covered vehicle speed range (km h^{-1})	Valid measurement period
2025-05-13	5–10	16:03–16:35
2025-05-14	5–20	14:47–16:18
2025-05-16	5–40	11:39–14:18
2025-05-17	5–40	11:38–15:22
2025-05-20	5–40	10:33–15:00
2025-05-21	5–40	10:24–15:01

S3 Regression analysis of the CFD simulation results under headwind and tailwind conditions

To examine the most basic linear response characteristics of the CFD-simulated flow distortion, bivariate linear regression models were fitted for v_{mx}, v_{my}, and Δv_z as functions of the inflow wind components v_{rx} and v_{ry}. The general form is written as

$$\hat{q} = a v_{rx} + b v_{ry} + c, \tag{S1}$$

where q denotes v_{mx}, v_{my}, or Δv_z, and $\hat{q}$ is the corresponding regression-based prediction.

Under headwind conditions, the fitted regression relationships are

$$\hat{v}_{mx} = 0.99\, v_{rx} + 0.08 v_{ry} - 0.01, \tag{S2}$$

$$\hat{v}_{my} = -0.02\, v_{rx} + 1.14 v_{ry}, \tag{S3}$$

$$\widehat{\Delta v_z} = 0.15\, v_{rx} - 0.06 v_{ry} + 0.01, \tag{S4}$$

Figures S3 presents comparisons between the regression-based predictions and the corresponding CFD simulation results under headwind conditions. The predicted values of the three velocity components exhibit very high levels of agreement with the CFD results. Both v_{mx} and v_{my} closely follow the ideal 1:1 relationship, while Δv_z also displays a stable linear response. The associated mean absolute error (MAE) and root mean square error (RMSE) remain at low levels. These results indicate that, under headwind conditions, the flow distortion structure is relatively simple, allowing a linear model to effectively capture its primary response characteristics.

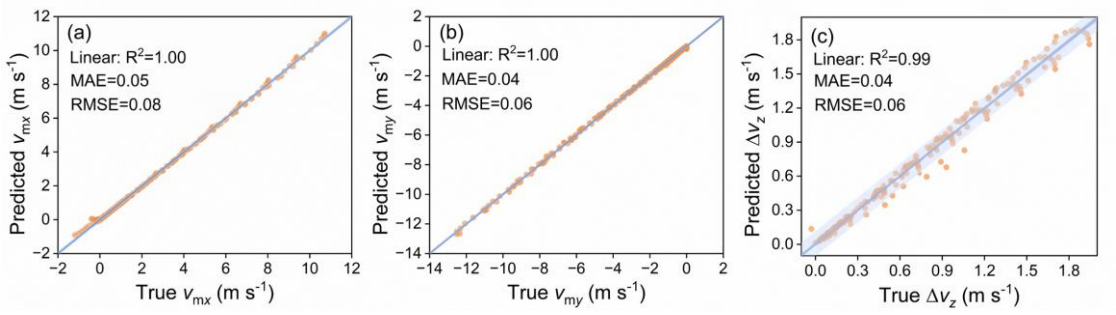

Figure S3: Bivariate linear regression analysis of the CFD simulation results under headwind conditions. The regression models are constructed with v_{mx}, v_{my}, and Δv_z as dependent variables and the inflow wind components v_{rx} and v_{ry} as independent variables. The solid blue line represents the fitted regression line. The dark blue shaded area denotes the 95% confidence interval, while the light blue shaded area indicates the 95% prediction interval. The grey 1:1 line represents the ideal prediction relationship.

Under tailwind conditions, the fitted regression relationships become

$$\hat{v}_{mx} = 0.88\, v_{rx} + 0.15 v_{ry} + 0.05, \tag{S5}$$

$$\hat{v}_{my} = 0.05\, v_{rx} + 1.16 v_{ry} + 0.04, \tag{S6}$$

$$\widehat{\Delta v_z} = 0.07\, v_{rx} - 0.15 v_{ry} + 0.01, \tag{S7}$$

By contrast, the fitting results for the tailwind conditions (Fig. S4) deteriorates compared to the headwind conditions, especially for the vertical wind velocity component. The predicted values of the three velocity components exhibit a much more scattered distribution, manifested in the substantially increased MAE and RMSE. Notably, the coefficient of determination (R^2) for Δv_z also decreases significantly, reaching only 0.67. This behaviour can be primarily attributed to the increased complexity of wake dominated nonlinear flow distortion under tailwind conditions, which cannot be adequately represented by a linear regression model.

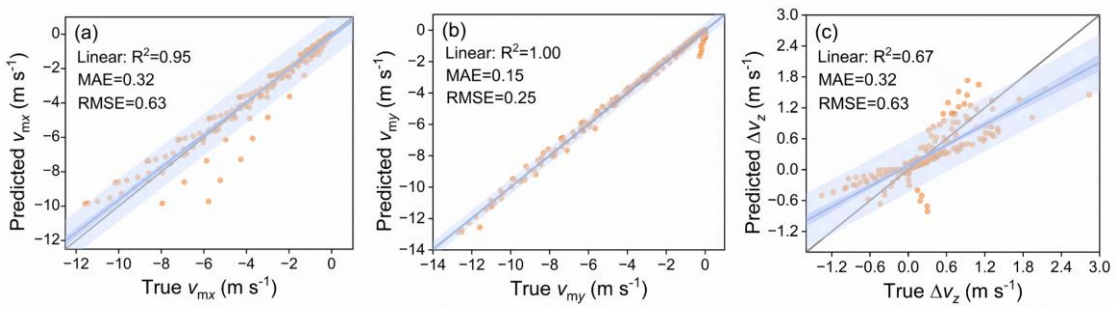

Figure S4: Bivariate linear regression analysis of the CFD simulation results under tailwind conditions. The regression models are constructed with v_{mx}, v_{my}, and Δv_z as dependent variables and the inflow wind components v_{rx} and v_{ry} as independent variables. The solid blue line represents the fitted regression line. The dark blue shaded area denotes the 95% confidence interval, while the light blue shaded area indicates the 95% prediction interval. The grey 1:1 line represents the ideal prediction relationship.

Taken together, these two sets of results indicate that flow distortion under headwind conditions exhibits more stable linear characteristics. Linear regression models therefore show higher applicability and predictive accuracy in this regime. In contrast, flow distortion under tailwind conditions is dominated by wake related effects and displays pronounced nonlinear behaviour. As a result, the applicability of linear models is limited, and more complex modelling approaches are required to further improve prediction performance. These findings provide an important basis for the development of the three-dimensional wind velocity correction algorithm.

S4 Derivation of the headwind flow distortion correction formulation

Equations (13)–(15) in the main text can be rewritten in matrix form as:

$$\begin{bmatrix} v_{mx}^{HW} \\ v_{my}^{HW} \\ \Delta v_z^{HW} \end{bmatrix} = \begin{bmatrix} 0.97 & 0 \\ 0 & 1.15 \\ 0.17 & 0 \end{bmatrix} \begin{bmatrix} v_{rx}^{HW} \\ v_{ry}^{HW} \end{bmatrix} + \begin{bmatrix} -0.18 \\ 0 \\ 0.13 \end{bmatrix}. \tag{S8}$$

In practical measurements, the vehicle-mounted anemometer directly provides the flow-distorted wind velocity components v_{mx}^{HW}, v_{my}^{HW}, and v_{mz}^{HW}. In the present formulation, the third relation is written in terms of Δv_z^{HW}, which is linked to v_{mz}^{HW} through

the disturbance definition given in the main text. Therefore, the true relative wind velocity vector $(v_{rx}^{HW}, v_{ry}^{HW}, v_{rz}^{HW})$ must be retrieved by inverting Eq. (S8). For convenience in the subsequent derivation, Eq. (S8) is rewritten as a linear mapping in matrix form:

$$\boldsymbol{y} = \boldsymbol{A}\boldsymbol{x} + \boldsymbol{b}, \tag{S9}$$

$$\boldsymbol{y} = \begin{bmatrix} v_{mx}^{HW} \\ v_{my}^{HW} \\ \Delta v_z^{HW} \end{bmatrix}, \tag{S10}$$

$$\boldsymbol{x} = \begin{bmatrix} v_{rx}^{HW} \\ v_{ry}^{HW} \end{bmatrix}, \tag{S11}$$

$$\boldsymbol{A} = \begin{bmatrix} 0.97 & 0 \\ 0 & 1.15 \\ 0.17 & 0 \end{bmatrix}, \tag{S12}$$

$$\boldsymbol{b} = \begin{bmatrix} -0.18 \\ 0 \\ 0.13 \end{bmatrix}. \tag{S13}$$

Equation (S9) represents an overdetermined linear system and therefore cannot be solved directly using a standard matrix inversion. In this study, a pseudo-inverse mapping is constructed using the least squares method (Ben-Israel and Greville, 2003). The true relative wind velocity is then retrieved by solving the least-squares problem in Eq. (S14).

$$\min_{\boldsymbol{x}} \|\boldsymbol{A}\,\boldsymbol{x} - (\boldsymbol{y} - \boldsymbol{b})\|^2 . \tag{S14}$$

The analytical solution of the inverse problem can be expressed as

$$\boldsymbol{x}^* = \boldsymbol{A}^+(\boldsymbol{y} - \boldsymbol{b}), \tag{S15}$$

where $\boldsymbol{x}^*$ denotes the optimal solution under the least squares criterion, and $\boldsymbol{A}^+$ represents the Moore–Penrose pseudo-inverse of matrix $\boldsymbol{A}$.

The analytical solution in Eq. (S15) can be further written in component form as follows:

$$v_{rx}^{HW} = 0.99\, v_{mx}^{HW} + 0.18\, v_{mz}^{HW} + 0.15, \tag{S16}$$

$$v_{ry}^{HW} = 0.87\, v_{my}^{HW}, \tag{S17}$$

$$v_{rz}^{HW} = v_{mz}^{HW} - \Delta v_z^{HW} = v_{mz}^{HW} - (0.17\, v_{mx}^{HW} + 0.031\, v_{mz}^{HW} + 0.13). \tag{S18}$$

To maintain consistency with the unified disturbance-based correction framework adopted in the main text, Eqs. (S16)–(S18) are further reformulated in terms of wind velocity disturbances as follows:

$$\Delta v_x^{HW} = v_{mx}^{HW} - v_{rx}^{HW} = -0.01\, v_{mx}^{HW} - 0.18\, v_{mz}^{HW} - 0.15, \tag{S19}$$

$$\Delta v_y^{HW} = v_{my}^{HW} - v_{ry}^{HW} = 0.13\, v_{my}^{HW}, \tag{S20}$$

$$\Delta v_z^{HW} = v_{mz}^{HW} - v_{rz}^{HW} = 0.17\, v_{mx}^{HW} + 0.031\, v_{mz}^{HW} + 0.13. \tag{S21}$$

S5 Derivation of the tailwind flow distortion correction formulation

Under tailwind conditions, the relative wind direction is defined in the vehicle coordinate system. The true relative wind direction and the measured distorted wind direction are expressed as

$$\beta_{\mathrm{r}}^{\mathrm{TW}} = \operatorname{actan}\left(\frac{v_{\mathrm{r}y}^{\mathrm{TW}}}{v_{\mathrm{r}x}^{\mathrm{TW}}}\right),\ \beta_{\mathrm{r}}^{\mathrm{TW}} \in (-\pi, \pi], \tag{S22}$$

$$\beta_{\mathrm{m}}^{\mathrm{TW}} = \operatorname{actan}\left(\frac{v_{\mathrm{m}y}^{\mathrm{TW}}}{v_{\mathrm{m}x}^{\mathrm{TW}}}\right),\ \beta_{\mathrm{m}}^{\mathrm{TW}} \in (-\pi, \pi], \tag{S23}$$

where $\beta_{\mathrm{r}}^{\mathrm{TW}}$ and $\beta_{\mathrm{m}}^{\mathrm{TW}}$ denote the true and measured relative wind directions, respectively. Both angles are expressed in radians (rad).

To avoid ambiguity associated with angle wrapping, the two-argument inverse tangent function (*atan2*) was used in the actual calculations. During the algorithm development, all wind direction angles were consistently represented in degrees (°). Based on this formulation, the quadratic polynomial mapping between the true relative wind direction and the measured disturbed wind direction can be expressed as:

$$\beta_{\mathrm{r}}^{\mathrm{TW}} = -56.81 + 0.039\,\beta_{\mathrm{m}}^{\mathrm{TW}} - 0.0040\,(\beta_{\mathrm{m}}^{\mathrm{TW}})^2. \tag{S24}$$

The component-wise disturbance quantities under tailwind conditions are defined as

$$\Delta v_x^{\mathrm{TW}} = v_{\mathrm{m}x}^{\mathrm{TW}} - v_{\mathrm{r}x}^{\mathrm{TW}}, \tag{S25}$$

$$\Delta v_y^{\mathrm{TW}} = v_{\mathrm{m}y}^{\mathrm{TW}} - v_{\mathrm{r}y}^{\mathrm{TW}}, \tag{S26}$$

$$\Delta v_z^{\mathrm{TW}} = v_{\mathrm{m}z}^{\mathrm{TW}} - v_{\mathrm{r}z}^{\mathrm{TW}}. \tag{S27}$$

After defining the wind direction mapping and the disturbance quantities, the next step is to establish functional relationships between the disturbance components Δv_x^{TW}, Δv_y^{TW}, and Δv_z^{TW} and the measured flow field characteristics as well as their derived variables. For the longitudinal and vertical disturbances (Δv_x^{TW} and Δv_z^{TW}), their variations are influenced not only by the projection of the inflow along the vehicle longitudinal direction but also by the lateral deflection angle and the wind speed magnitude. Based on these considerations, the longitudinal measured wind component $v_{\mathrm{m}x}^{\mathrm{TW}}$, the absolute value of the lateral wind component $\left|v_{\mathrm{m}y}^{\mathrm{TW}}\right|$, the relative wind direction $\beta_{\mathrm{r}}^{\mathrm{TW}}$ obtained from the wind direction mapping (calculated using Eq. (S24)), and the measured horizontal wind speed magnitude $V_{\mathrm{m}}^{\mathrm{TW}}$ (see Eq. (S28)) are selected as input features for the disturbance model.

$$V_{\mathrm{m}}^{\mathrm{TW}} = \sqrt{(v_{\mathrm{m}x}^{\mathrm{TW}})^2 + (v_{\mathrm{m}y}^{\mathrm{TW}})^2}\,. \tag{S28}$$

By comparison, the lateral disturbance Δv_y^{TW} under tailwind conditions mainly manifests as a scaling effect in the lateral direction, characterized by either amplification or attenuation. Its variation shows a strong correlation with the measured lateral wind component itself. Therefore, in this study, only the measured longitudinal and lateral wind components, $v_{\mathrm{m}x}^{\mathrm{TW}}$ and $v_{\mathrm{m}y}^{\mathrm{TW}}$, are used as input features to model Δv_y^{TW}.

Based on the above features, a second-order polynomial model is used to parameterize each disturbance component. The general form can be written as:

$$\Delta v_i^{\mathrm{TW}} = f_i^{\mathrm{TW}}(\boldsymbol{\xi}) = a_0{}^{(i)} + \sum_{j=1}^{n} a_j{}^{(i)}\xi_j + \sum_{j=1}^{n}\sum_{k=j}^{n} a_{jk}^{(i)}\xi_j\xi_k, \qquad i \in \{x, y, z\} \tag{S29}$$

where $\boldsymbol{\xi} = (\xi_1, \xi_2, \ldots, \xi_n)$ denotes the input feature vector corresponding to each disturbance component; The index $i \in \{x, y, z\}$ indicates the disturbance direction, corresponding to the longitudinal, lateral, and vertical directions in the vehicle coordinate system, respectively. $a_0^{(i)}$, $a_j^{(i)}$, and $a_{jk}^{(i)}$ are the model parameters obtained by regression, and n is the number of input features.

The final model achieves R^2 of 0.99, 0.99, and 0.85 in the x-, y-, and z-directions, respectively. To enhance the interpretability of the model, the contributions of individual terms in the second-order polynomial formulation are further analyzed. By evaluating the relative importance of each polynomial term in the prediction results, the key terms that play a dominant role in the model fitting are identified. An explained-variance threshold of 90% is then applied, based on which the dominant contributing terms are retained. It should be noted that the complete second-order polynomial model is still used in the actual wind speed correction in order to preserve prediction accuracy. Based on the above formulation, the disturbance correction algorithm under tailwind conditions is obtained as follows:

$$\Delta v_x^{\mathrm{TW}} \approx -0.28 + 3.42\left|v_{\mathrm{m}y}^{\mathrm{TW}}\right| + 0.37\,(V_{\mathrm{m}}^{\mathrm{TW}})^2 + V_{\mathrm{m}}^{\mathrm{TW}}\left(-4.68 + 0.70\,v_{\mathrm{m}x}^{\mathrm{TW}} - 0.43\left|v_{\mathrm{m}y}^{\mathrm{TW}}\right| - 0.046\,\beta_{\mathrm{r}}^{\mathrm{TW}}\right), \tag{S30}$$

$$\Delta v_y^{\mathrm{TW}} = 0.095\,v_{\mathrm{m}y}^{\mathrm{TW}} - 0.015\,v_{\mathrm{m}x}^{\mathrm{TW}} v_{\mathrm{m}y}^{\mathrm{TW}}, \tag{S31}$$

$$\Delta v_z^{\mathrm{TW}} \approx -0.11 + 2.04\left|v_{\mathrm{m}y}^{\mathrm{TW}}\right| - 1.72\,v_{\mathrm{m}x}^{\mathrm{TW}} + V_{\mathrm{m}}^{\mathrm{TW}}(-2.43 + 0.13\,v_{\mathrm{m}x}^{\mathrm{TW}} - 0.018\,\beta_{\mathrm{r}}^{\mathrm{TW}}) + \beta_{\mathrm{r}}^{\mathrm{TW}}\left(-0.014\,v_{\mathrm{m}x}^{\mathrm{TW}} + 0.013\left|v_{\mathrm{m}y}^{\mathrm{TW}}\right|\right). \tag{S32}$$

The true relative wind velocity under tailwind conditions is then recovered from

$$\begin{bmatrix} v_{\mathrm{r}x}^{\mathrm{TW}} \\ v_{\mathrm{r}y}^{\mathrm{TW}} \\ v_{\mathrm{r}z}^{\mathrm{TW}} \end{bmatrix} = \begin{bmatrix} v_{\mathrm{m}x}^{\mathrm{TW}} \\ v_{\mathrm{m}y}^{\mathrm{TW}} \\ v_{\mathrm{m}z}^{\mathrm{TW}} \end{bmatrix} - \begin{bmatrix} \Delta v_x^{\mathrm{TW}} \\ \Delta v_y^{\mathrm{TW}} \\ \Delta v_z^{\mathrm{TW}} \end{bmatrix}. \tag{S33}$$

References

Ben-Israel, A. and Greville, T. N.: Generalized inverses: theory and applications, Springer, 2003.